

FLUX-TRANSPORT DYNAMOS WITH LORENTZ FORCE FEEDBACK ON DIFFERENTIAL ROTATION AND MERIDIONAL FLOW: SATURATION MECHANISM AND TORSIONAL OSCILLATIONS

MATTHIAS REMPEL

High Altitude Observatory, National Center for Atmospheric Research* , P.O. Box 3000, Boulder, Colorado 80307, USA
Draft version October 19, 2018

ABSTRACT

In this paper we discuss a dynamic flux-transport dynamo model that includes the feedback of the induced magnetic field on differential rotation and meridional flow. We consider two different approaches for the feedback: mean field Lorentz force and quenching of transport coefficients such as turbulent viscosity and heat conductivity. We find that even strong feedback on the meridional flow does not change the character of the flux-transport dynamo significantly; however it leads to a significant reduction of differential rotation. To a large degree independent from the dynamo parameters, the saturation takes place when the toroidal field at the base of the convection zone reaches between 1.2 and 1.5 T, the energy converted into magnetic energy corresponds to about 0.1% to 0.2% of the solar luminosity. The torsional oscillations produced through Lorentz force feedback on differential rotation show a dominant poleward propagating branch with the correct phase relation to the magnetic cycle. We show that incorporating enhanced surface cooling of the active region belt (as proposed by Spruit) leads to an equatorward propagating branch in good agreement with observations.

Subject headings: Sun: interior — rotation — magnetic field — dynamo

1. INTRODUCTION

Flux-transport dynamos have proven to be successful for modeling the evolution of the large scale solar magnetic field (Wang & Sheeley 1991; Durney 1995; Choudhuri et al. 1995; Dikpati & Charbonneau 1999; Küker et al. 2001; Dikpati & Gilman 2001; Dikpati et al. 2004; Dikpati 2005; Dikpati et al. 2006). In a flux-transport dynamo the equatorward propagation of the magnetic activity belt (butterfly diagram) is a consequence of the equatorward transport of magnetic field at the base of the convection zone by the meridional flow.

However, all studies so far have addressed the transport of magnetic field by the meridional circulation in a purely kinematic regime. The toroidal field strength at the base of the solar convection zone inferred from studies of rising magnetic flux tubes (Choudhuri & Gilman 1987; Fan et al. 1993; Schüssler et al. 1994; Caligari et al. 1995, 1998) is around 10 T (100 kG) and thus orders of magnitude larger than the equipartition field strength estimated from a meridional flow velocity of a few m s^{-1} . Therefore it is crucial for flux-transport dynamos to include the feedback of the Lorentz force on the meridional flow.

In order to be able to address this question it is necessary to incorporate a model for the solar differential rotation and meridional flow into a dynamo model and allow for the feedback of the Lorentz force on differential rotation and meridional flow. Differential rotation and meridional flow have been addressed in the past mainly through two approaches: 3D full spherical shell simulations (Glatzmaier & Gilman 1982; Gilman & Miller 1986; Miesch et al. 2000; Brun & Toomre 2002) and axisymmetric mean field models (Kitchatinov & Rüdiger 1993, 1995; Rüdiger et al. 1998; Küker & Stix 2001). While the 3D simulations have trouble reproducing a

consistent large scale meridional flow pattern (poleward in the upper half of the convection zone), as it is inferred by helioseismology (Braun & Fan 1998; Haber et al. 2002; Zhao & Kosovichev 2004), such a flow is a common feature in most of the mean field models.

In this paper we build upon the differential rotation model presented in Rempel (2005b) and combine it with the axisymmetric mean field dynamo equations. The magnetic field is allowed to feed back on differential rotation and meridional flow through the mean field Lorentz force and quenching of turbulent viscosity and heat conductivity. We have addressed already in a previous paper (Rempel 2006) the feedback of magnetic field on the meridional flow by imposing a static toroidal magnetic and including magnetic tension and quenching of turbulent viscosity in the differential rotation model. We found that a significant feedback can be expected if the toroidal magnetic field strength is around 3 T or above equipartition. In this paper we do not impose a toroidal field, but rather solve the induction equation to obtain a time dependent magnetic field. Going beyond Rempel (2006), we also include the feedback on differential rotation leading to a solar cycle variation of the rotation rate, which is known as torsional oscillations (Howard & Labonte 1980; Toomre et al. 2000; Howe et al. 2000; Antia & Basu 2001; Vorontsov et al. 2002; Howe et al. 2005).

A very similar approach was taken before by Brandenburg et al. (1990, 1991, 1992). In their model they were solving a mean field differential rotation model parallel to the dynamo equation to obtain a 'dynamic' dynamo. The main difference in our approach is that we focus on flux-transport dynamos, whereas their work described mainly $\alpha\Omega$ -dynamos with the advection of field by a meridional flow playing only a secondary role. Given recent developments in solar dynamo theory, showing that flux transport dynamos are very successful in reproducing most of the observed features (Dikpati 2005) it

*The National Center for Atmospheric Research is sponsored by the National Science Foundation
Electronic address: rempel@hao.ucar.edu

is important to evaluate to which degree these dynamos change operation if dynamic feedback is considered.

Lorentz force feedback has been considered in mean field dynamo models in various levels of sophistication:

Küker et al. (1999) used a model including both macro (mean field Lorentz force) and micro (quenching of Λ -effect) feedback to evaluate to which extent grand minima can be produced through feedback on differential rotation.

Covas et al. (2000, 2004, 2005) considered feedback on differential rotation in a classical $\alpha\Omega$ -dynamo model solving a simplified momentum equation including the mean field Lorentz force and a diffusive relaxation term for the longitudinal flow velocity perturbation. They were able to reproduce the basic features of the observed solar torsional oscillation pattern (equatorward and poleward propagating branch). A similar approach has been taken before by Moss & Brooke (2000); Tobias (1996); Yoshimura (1981).

In contrast to this the models of Schüssler (1979); Brandenburg et al. (1990, 1991, 1992); Jennings (1993); Moss et al. (1995); Muhli et al. (1995) incorporate the full momentum equation, allowing also for magnetically driven meridional motions. The main focus of their work was on understanding the non-linear saturation of the dynamo.

The consideration of the macroscopic mean field Lorentz force, common for all models listed above, is also known in the literature as 'Malkus-Proctor-effect' (Malkus & Proctor 1975).

A different approach has been used by Kitchatinov & Pipin (1998) and Kitchatinov et al. (1999), who considered feedback through quenching of the Λ -effect (turbulent angular momentum transport driving differential rotation). Their work focused on understanding torsional oscillations as well as the possibility of producing grand activity cycles through this type of feedback.

This paper is organized as follows: In section 2 we explain the physics included in the non-kinematic dynamo model. Section 3 shows the results of the non-kinematic dynamo runs including a detailed analysis of the energy flows within the model. Section 4 focuses on the properties of the torsional oscillations produced by the model and compares them to results obtained by helioseismology. Section 5 discusses the choices we make for various parameters of the mean field model and their impact on the solutions presented here. In section 6 we summarize the main results of this investigation and discuss them in the context of solar dynamo models.

2. MODEL

In this paper we utilize the mean field differential rotation and meridional circulation model of Rempel (2005b) and couple it with the axisymmetric mean field dynamo equations. The computed differential rotation and meridional flow are used to advance the magnetic field by using a Babcock-Leighton flux transport dynamo model. The computed magnetic field is allowed to feed back on differential rotation and meridional flow through the Lorentz force and quenching of turbulent viscosity and thermal heat conductivity. We are solving the axisymmetric MHD equations including parameterizations of processes on the (unresolved) convective scale (mean

field approach). We introduce in the induction equation the vector potential for the poloidal field to satisfy the constraint $\nabla \cdot \mathbf{B} = 0$.

$$\frac{\partial \varrho_1}{\partial t} = -\frac{1}{r^2} \frac{\partial}{\partial r} (r^2 v_r \varrho_0) - \frac{1}{r \sin \theta} \frac{\partial}{\partial \theta} (\sin \theta v_\theta \varrho_0) \quad (1)$$

$$\begin{aligned} \frac{\partial v_r}{\partial t} = & -v_r \frac{\partial v_r}{\partial r} - \frac{v_\theta}{r} \frac{\partial v_r}{\partial \theta} + \frac{v_\theta^2}{r} - \frac{\partial}{\partial r} \frac{p_{\text{tot}}}{\varrho_0} + \frac{p_{\text{mag}}}{\gamma p_0} g + \frac{s_1}{\gamma} g \\ & + (2\Omega_0 \Omega_1 + \Omega_1^2) r \sin^2 \theta + \frac{1}{\varrho_0} (F_r^\nu + F_r^B) \quad (2) \end{aligned}$$

$$\begin{aligned} \frac{\partial v_\theta}{\partial t} = & -v_r \frac{\partial v_\theta}{\partial r} - \frac{v_\theta}{r} \frac{\partial v_\theta}{\partial \theta} - \frac{v_r v_\theta}{r} - \frac{1}{r} \frac{\partial}{\partial \theta} \frac{p_{\text{tot}}}{\varrho_0} \\ & + (2\Omega_0 \Omega_1 + \Omega_1^2) r \sin \theta \cos \theta + \frac{1}{\varrho_0} (F_\theta^\nu + F_\theta^B) \quad (3) \end{aligned}$$

$$\begin{aligned} \frac{\partial \Omega_1}{\partial t} = & -\frac{v_r}{r^2} \frac{\partial}{\partial r} [r^2 (\Omega_0 + \Omega_1)] \\ & - \frac{v_\theta}{r \sin^2 \theta} \frac{\partial}{\partial \theta} [\sin^2 \theta (\Omega_0 + \Omega_1)] \\ & + \frac{1}{\varrho_0 r \sin \theta} (F_\phi^\nu + F_\phi^B) \quad (4) \end{aligned}$$

$$\begin{aligned} \frac{\partial s_1}{\partial t} = & -v_r \frac{\partial s_1}{\partial r} - \frac{v_\theta}{r} \frac{\partial s_1}{\partial \theta} + v_r \frac{\gamma \delta}{H_p} + \frac{\gamma - 1}{p_0} Q \\ & + \frac{1}{\varrho_0 T_0} \nabla \cdot (\kappa_t \varrho_0 T_0 \nabla s_1) + \frac{\gamma - 1}{p_0} \eta_t (\nabla \times \mathbf{B})^2 \quad (5) \end{aligned}$$

$$\begin{aligned} \frac{\partial B_\Phi}{\partial t} = & -\frac{1}{r} \frac{\partial}{\partial r} (r v_r B_\Phi) - \frac{1}{r} \frac{\partial}{\partial \theta} (v_\theta B_\Phi) + r \sin \theta B_r \frac{\partial \Omega_1}{\partial r} \\ & + \sin \theta B_\theta \frac{\partial \Omega_1}{\partial \theta} + \eta_t \left(\Delta - \frac{1}{(r \sin \theta)^2} \right) B_\Phi \\ & + \frac{1}{r} \frac{\partial \eta_t}{\partial r} \frac{\partial}{\partial r} (r B_\Phi) + \frac{1}{r^2} \frac{\partial \eta_t}{\partial \theta} \frac{1}{\sin \theta} \frac{\partial}{\partial \theta} (\sin \theta B_\Phi) \quad (6) \end{aligned}$$

$$\begin{aligned} \frac{\partial A}{\partial t} = & -\frac{v_r}{r} \frac{\partial}{\partial r} (r A) - \frac{v_\theta}{r \sin \theta} \frac{\partial}{\partial \theta} (\sin \theta A) \\ & + \eta_t \left(\Delta - \frac{1}{(r \sin \theta)^2} \right) A + S(r, \theta, B_\Phi) . \quad (7) \end{aligned}$$

Here ϱ_0 and p_0 denote the (spherical symmetric) reference state stratification, $H_p = p_0/(\varrho_0 g)$ the pressure scale height, ϱ_1 and p_1 perturbations around the reference state caused by differential rotation and meridional flow. Since these perturbations are small compared to the reference state values, the equations are linearized assuming $\varrho_1 \ll \varrho_0$ and $p_1 \ll p_0$. Ω_0 denotes the rotation rate of the core, Ω_1 the differential rotation with respect to the core in the convection zone. The quantity $s_1 = p_1/p_0 - \gamma \varrho_1/\varrho_0$ denotes the dimensionless entropy perturbation (normalized by the heat capacity c_v). For the reference state we use an adiabatic polytrope assuming a gravity varying $\sim r^{-2}$; however, small perturbations from adiabaticity are considered in the entropy equation through the third term $\sim \delta = \nabla - \nabla_{\text{ad}}$. The quantity p_{mag} denotes the magnetic pressure, $p_{\text{tot}} = p_1 + p_{\text{mag}}$ the total pressure. The buoyancy term in Eq. (2) has been written in a way to separate the magnetic buoyancy from non-magnetic buoyancy, assuming $|\nabla - \nabla_{\text{ad}}| \ll 1$. Since the most unstable modes driven by magnetic buoyancy are typically non-axisymmetric, the description of magnetic buoyancy in our axisymmetric model is not necessarily very realistic. Therefore we will discuss later also simulations with mag-

netic buoyancy switched off by ignoring the term $\sim p_{\text{mag}}$ in Eq. (2).

The quantity $\mathbf{F}^B = 1/\mu_0 \nabla \cdot (\mathbf{B}\mathbf{B})$ denotes magnetic tension, where the poloidal magnetic field follows from the vector potential A used in Eq. (7) through

$$B_r = \frac{1}{r \sin \theta} \frac{\partial}{\partial \theta} (\sin \theta A) \quad (8)$$

$$B_\theta = -\frac{1}{r} \frac{\partial}{\partial r} (rA) . \quad (9)$$

For computing the Lorentz force we consider here only the magnetic mean field contribution. Formally an additional contribution to the stress tensor $\sim \langle \mathbf{B}'\mathbf{B}' \rangle$ caused by the turbulent magnetic field exists; however the contribution of these terms in detail is not well understood. We emphasize that considering only the mean field Lorentz force leads to a model that is energetically consistent in the way that the energy extracted from differential rotation and meridional flow is flowing into the reservoir of magnetic energy via the induction equation. Considering additional Lorentz force terms in the momentum equation requires that these terms only redistribute momentum (otherwise additional terms in the induction equation would be required as well to be energetically consistent). This effect referred to as viscoelasticity by some authors (Longcope et al. 2003) could be parametrized to some extent as an additional source of viscous stress. Another possible feedback of these terms is quenching of turbulent transport processes such as turbulent angular momentum transport, viscosity and heat conductivity, which we will consider later in the form:

$$\nu_t = \frac{\nu_t^0}{1 + (B/B_{\text{eq}})^2} \quad (10)$$

$$\kappa_t = \frac{\kappa_t^0}{1 + (B/B_{\text{eq}})^2} \quad (11)$$

The quantity \mathbf{F}^ν denotes turbulent viscous stresses, including turbulent transport of angular momentum (Λ -effect), Q considers the associated viscous dissipation in the entropy equation. In our model the Λ -effect is the primary driver of differential rotation and meridional flow, while the profile of the differential rotation (the deviation from the Taylor-Proudman state) is a consequence of a latitudinal entropy gradient. The latitudinal entropy gradient follows in our model self consistently from the inclusion of a subadiabatic tachocline. For further details concerning the differential rotation model we refer to Rempel (2005b) and section 2.1.

Eqs. (6) and (7) are the axisymmetric mean field dynamo equation, including transport of magnetic field by meridional flow, shear by differential rotation, magnetic diffusion and induction by a Babcock-Leighton surface α -effect, parametrized through the poloidal source term $S(r, \theta, B_\Phi)$. We will discuss the dynamo model in more detail in section 2.2.

For the solar parameter range the system defined by Eqs. (1) - (7) is in the regime of highly subsonic flows, which introduces a significant CFL time step constraint if solved explicitly. We do not use here the anelastic approximation as many others do; instead we use an approach of artificially reducing the speed of sound to values that do not impose a significant time step constraint

(compared to the diffusive time step) but still ensure that the flows remain highly subsonic. Given the fact that the Mach number of the meridional flow in the bulk of the convection zone is around 10^{-5} a decrease of the speed of sound by a factor ~ 100 is found to have no impact on the solution and is used for most of the results shown. Formally this is achieved by changing the equation of continuity to

$$\frac{\partial \varrho_1}{\partial t} = -\zeta^2 \left[\frac{1}{r^2} \frac{\partial}{\partial r} (r^2 v_r \varrho_0) - \frac{1}{r \sin \theta} \frac{\partial}{\partial \theta} (\sin \theta v_\theta \varrho_0) \right] \quad (12)$$

with $\zeta \sim 0.01$, which reduces the speed of sound by a factor ζ . This approach is equivalent to increasing the base rotation rate and scaling up all other variables to maintain the proper relations between the different terms in the equations (Rempel 2005b). The modified equations are solved using a MacCormack scheme. We emphasize that this approach is only feasible for the axisymmetric system, where the much faster speed of rotation does not enter the CFL condition.

2.1. Differential rotation, meridional flow reference model

In this paper we use a reference model that is very close to model 1 discussed in Rempel (2005b). We made the following changes in order to obtain a meridional flow pattern that leads to a solar like dynamo period and a confinement of magnetic activity close to the equator: We use a value of the parameter n defining the latitudinal profile of the Λ -effect of 3, an amplitude of the Λ -effect of $\Lambda_0 = 1$, and a value of turbulent viscosity and heat conductivity of $3 \times 10^8 \text{ m}^2 \text{ s}^{-1}$. Λ_0 determines primarily the amplitude of differential rotation, while a change of ν_t and κ_t (keeping ν_t/κ_t constant) adjusts the meridional flow speed.

Fig. 1 a,b) shows the differential rotation and Fig. 1 c,d) the meridional flow of the reference model. Note that in our model most of the radial shear is located beneath the base of the convection zone $r_{\text{bc}} = 0.71 R_\odot$. This is due to the fact that the differential rotation is driven by the Λ -effect within the convection and uniform rotation is imposed at the lower boundary at $r = 0.65 R_\odot$. As a consequence a viscous shear layer forms between both regions, which has the largest shear rate where the turbulent viscosity is assumed to be small (below r_{bc}). Also the meridional flow does not show a significant penetration below r_{bc} , due to the subadiabatic stratification and the significant drop of turbulent viscosity (see Rempel (2005b) for a detailed discussion).

2.2. Flux-transport dynamo model

We use a flux-transport dynamo model similar to the approach of Dikpati & Charbonneau (1999), except for the fact that differential rotation and meridional flow are not prescribed, but computed by the model described above. The additional dynamo parameters we have to specify are the profile of the magnetic diffusivity η_t and the functional form of the poloidal source term $S(r, \theta, B_\Phi)$ in Eq. 7. The turbulent magnetic diffusivity η_t is specified as function in radius, given by

$$\eta_t = \eta_c + f_c(r) [\eta_{\text{bc}} - \eta_c + f_{cz}(r) (\eta_{cz} - \eta_{\text{bc}})] \quad (13)$$

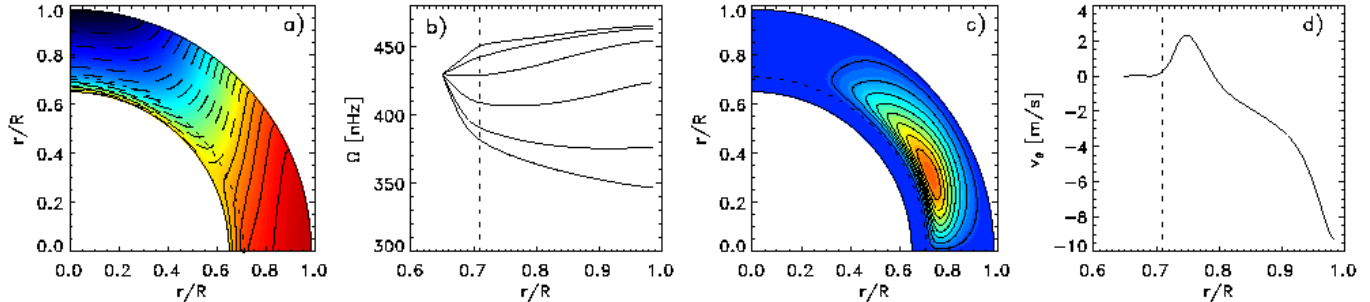


FIG. 1.— Differential rotation and meridional flow of the reference model. a) Contours of Ω , b) radial profiles of Ω for the latitudes (top to bottom) 0° , 15° , 30° , 45° , 60° , and 90° . c) shows the stream function of the meridional flow, d) the flow profile at 30° latitude. The dotted line indicates the base of the convection zone at $r_{bc} = 0.71 R_\odot$. Note that in our model most of the radial shear is located beneath r_{bc} , while the meridional flow shows only very little penetration beneath r_{bc} .

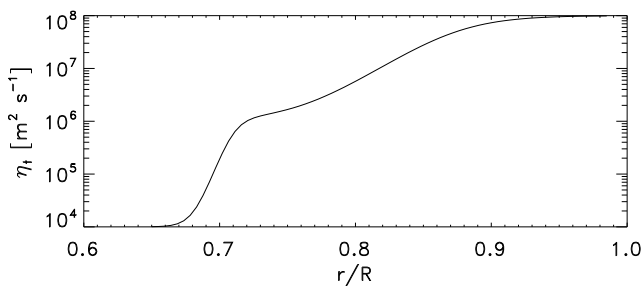


FIG. 2.— Profile of η_t used for the dynamo simulation. η_t drops by two orders of magnitude within the convection starting from a surface value of $10^8 \text{ m}^2 \text{ s}^{-1}$. There is an additional drop by one order of magnitude beneath the base of the convection zone.

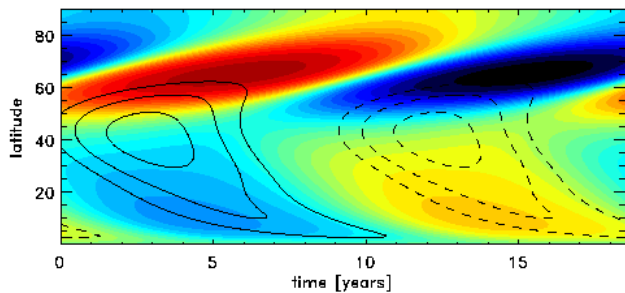


FIG. 3.— Butterfly diagram of toroidal magnetic field (contour lines of $\bar{B}_{\Phi, bc}$) and radial field close to surface $r = 0.985 R_\odot$ (color shades). The maximum field strength of B_Φ is 1.28 T, the maximum field strength of B_r is 0.01 T.

with

$$f_{cz}(r) = \frac{1}{2} \left[1 + \tanh \left(\frac{r - r_{cz}}{d_{cz}} \right) \right] \quad (14)$$

$$f_c(r) = \frac{1}{2} \left[1 + \tanh \left(\frac{r - r_{bc}}{d_{bc}} \right) \right]. \quad (15)$$

The function $f_{cz}(r)$ determines the profile within the convection zone, while $f_c(r)$ ensures a significant drop of η_t beneath r_{bc} . η_c determines the core diffusivity, η_{bc} the diffusivity at the base of the convection zone, and η_{cz} the diffusivity in the upper half of the convection zone. For this discussion we use a profile with the parameters

$\eta_c = 10^5 \text{ m}^2 \text{ s}^{-1}$, $\eta_{bc} = 10^6 \text{ m}^2 \text{ s}^{-1}$, $\eta_{cz} = 10^8 \text{ m}^2 \text{ s}^{-1}$, $r_{cz} = 0.875 R_\odot$, $d_{cz} = 0.05 R_\odot$, $r_{bc} = 0.71 R_\odot$, $d_{bc} = 0.0125 R_\odot$. The profile is shown in Fig. 2. We use here for reasons of numerical stability a value of η_c that is significantly larger than molecular resistivity. However, the influence of η_c on the solution is found to be very weak.

Our model uses a non-local Babcock-Leighton α -effect (Babcock 1961; Leighton 1969) in which the source term $S(r, \theta, B_\Phi)$ at the surface is dependent on the toroidal field strength at the base of the convection zone averaged over the interval $[0.71 R_\odot, 0.76 R_\odot]$, $\bar{B}_{\Phi, bc}$. The functional form of S is then

$$S(r, \theta, B_\Phi) = \alpha_0 \bar{B}_{\Phi, bc}(\theta) f_\alpha(r) g_\alpha(\theta), \quad (16)$$

with

$$f_\alpha(r) = \max \left[0, 1 - \frac{(r - r_{\max})^2}{d_\alpha^2} \right] \quad (17)$$

$$g_\alpha(\theta) = \frac{(\sin \theta)^2 \cos \theta}{\max [(\sin \theta)^2 \cos \theta]} \quad (18)$$

$$\bar{B}_{\Phi, bc}(\theta) = \int_{r_{\min}}^{r_{\max}} dr h(r) B_\Phi(r, \theta). \quad (19)$$

We use here $d_\alpha = 0.05 R_\odot$, which confines the poloidal source term above $r = 0.935 R_\odot$, peaking at r_{\max} . The function $h(r)$ is an averaging kernel with $\int_{r_{\min}}^{r_{\max}} dr h(r) = 1$. We use a parabolic profile vanishing at $0.71 R_\odot$ and $0.76 R_\odot$ with peak at $0.735 R_\odot$.

The boundary condition is $A = B_\Phi = 0$ at the pole and $\partial A / \partial \theta = B_\Phi = 0$ at the equator, which selects the dipole symmetry for the solution. B_Φ vanishes at both radial boundaries. A vanishes at the inner boundary and the poloidal field is assumed to be radial at the top boundary. The dynamo part of our code has been compared intensively with the code of Dikpati & Charbonneau (1999).

We emphasize that the main goal of this paper is a fundamental understanding of dynamical effects caused by the feedback of the dynamo generated field on differential rotation and meridional flow, rather than a detailed model of the solar dynamo. We have chosen the dynamo parameters and the parameters of differential rotation model such that the solutions show a reasonable, but not detailed agreement in terms of butterfly diagram and dynamo period as well as amplitude of differential

rotation and meridional flow with observations. We restrict our simulations to one hemisphere and impose the dipole symmetry through our equatorial boundary condition. We do not try to address the parity issue in this model, which has been done for flux-transport dynamo by Dikpati & Gilman (2001).

Before we discuss dynamic solutions, we present here as reference a kinematic dynamo solution computed with the differential rotation and meridional flow shown in Fig. 1. We use for the α -effect and amplitude of $\alpha_0 = 0.125 \text{ ms}^{-1}$ and include α -quenching with a quenching field strength of 1 T (10 kG). The butterfly diagram computed from the averaged toroidal field ($\bar{B}_{\Phi, \text{bc}}$) and the radial field at the 'surface' $r = 0.985 R_{\odot}$ is shown in Fig. 3. The dynamo period for this setup is around 19 years, the maximum toroidal field at $r = 0.735 R_{\odot}$ is 1.28 T, the maximum field strength of the radial field at $r = 0.985 R_{\odot}$ is 0.01 T.

The butterfly diagram shows equatorward propagating activity belts starting around 50° latitude and having their peak field strength at around 40° latitude. The polar reversal of the poloidal field takes place during maximum activity with the toroidal field in low latitudes, changing sign from negative to positive while the low latitude toroidal field is positive as found in observations.

3. DYNAMO MODEL WITH LORENTZ FORCE FEEDBACK

3.1. General solution properties

In this section we discuss results obtained with full Lorentz force feedback on differential rotation and meridional flow. Since Lorentz force feedback introduces enough non-linearity to saturate the dynamo, it is not necessary to include α -quenching as typically done in kinematic models. We present here three models varying the value of the α -effect in order to show different regimes in terms of intensity of the Lorentz force feedback. The α_0 values used are 0.125, 0.25, and 0.5 ms^{-1} . We also present results computed from a model with a magnetic diffusivity reduced in the bulk of the convection zone from $\eta_{\text{cz}} = 10^8 \text{ m}^2 \text{ s}^{-1}$ to $\eta_{\text{cz}} = 5 \times 10^7 \text{ m}^2 \text{ s}^{-1}$.

Figure 4 shows the model with $\alpha_0 = 0.125 \text{ ms}^{-1}$. The top panel displays the radial magnetic field close to the surface ($r = 0.985 R_{\odot}$), the middle panel the meridional flow at $r = 0.735 R_{\odot}$, and the bottom panel the torsional oscillations at $r = 0.985 R_{\odot}$. In all three panels the toroidal field contours at $r = 0.735 R_{\odot}$ are indicated (solid: positive values, dashed: negative values). Compared to Figure 3 the butterfly diagram shows major distortions caused by magnetic buoyancy breaking up the layer of toroidal field at the base of the convection zone. We present a more detailed discussion of the role of magnetic buoyancy in subsection 3.4. The radial surface field is close to that in Figure 3. The equatorward meridional flow at $r = 0.735 R_{\odot}$ shows a variation of around 30% of the mean flow amplitude (around 2 ms^{-1}) in anti-phase with the toroidal field intensity, caused by the influence of the magnetic tension of the toroidal field. This feedback is not strong enough to switch off the equatorward transport of magnetic field and therefore does not influence the flux transport dynamo significantly. This is in agreement with Rempel (2006), who found that equatorward transport of toroidal field is possible up to around 3 T. The bottom panel of Figure 4 shows the temporal variation of the differential rotation caused by the

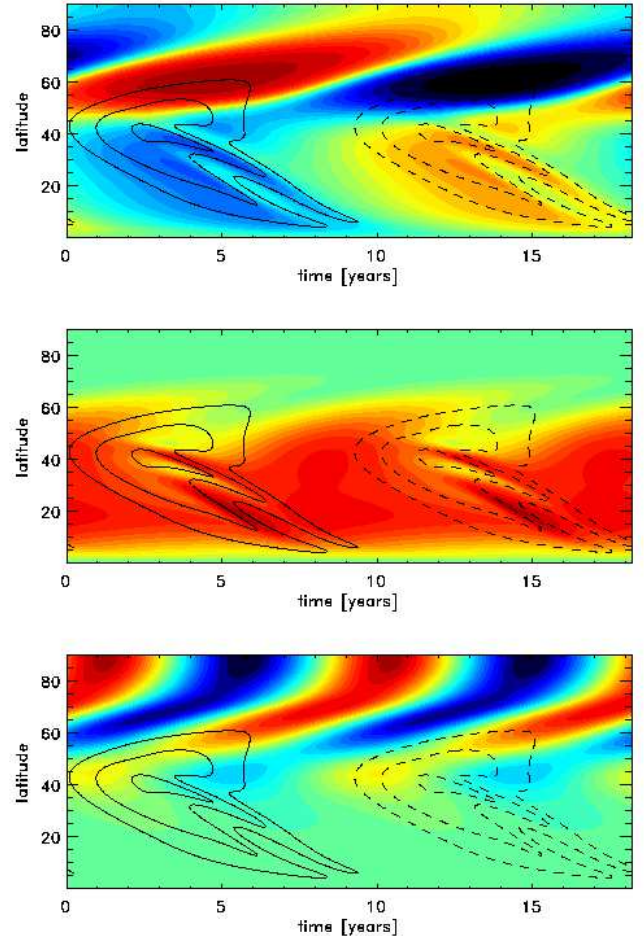


FIG. 4.— Dynamo solution with Lorentz force feedback and no α -quenching. All dynamo parameters are the same as for the reference solution (with α -quenching) shown in Fig. (3). Top panel: Butterfly diagram of toroidal magnetic field (contour lines) and radial field close to surface $r = 0.985 R_{\odot}$ (color shades). The maximum toroidal field strength is 1.17 T, the maximum radial field strength at the surface is 0.014 T. Middle panel: Meridional flow (v_{θ} , color shades) at $r = 0.75 R_{\odot}$. The maximum flow velocity is 2.27 ms^{-1} . Bottom Panel: Torsional oscillation pattern ($\Omega - \bar{\Omega}$) at $r = 0.985 R_{\odot}$. The maximum amplitude is 1% of the core rotation rate corresponding to a variation of about 4 nHz. The torsional oscillation pattern at $r = 0.735 R_{\odot}$ is very similar, but has a slightly reduced amplitude.

Lorentz force feedback, also known as torsional oscillations. We find in our model mainly a poleward propagating oscillation pattern, starting at mid latitudes. The amplitude close to the surface is around 1% of the core rotation rate, which corresponds to roughly 4 nHz. We discuss torsional oscillations in detail in section 4.

Fig. 5 shows 3 snapshots of the magnetic field (field lines of poloidal field and toroidal field strength as color shades), corresponding to $t = 0$, $t = 3.25$ and $t = 6.5$ years in Fig. 4. The middle and bottom panel show the breakup of the magnetic layer caused by magnetic buoyancy force.

Fig. 6 shows the dynamo solution (butterfly diagram and radial field close to surface) for the cases with increasing value of α_0 . In a kinematic model with α -quenching as non-linearity, an increase of α increases the

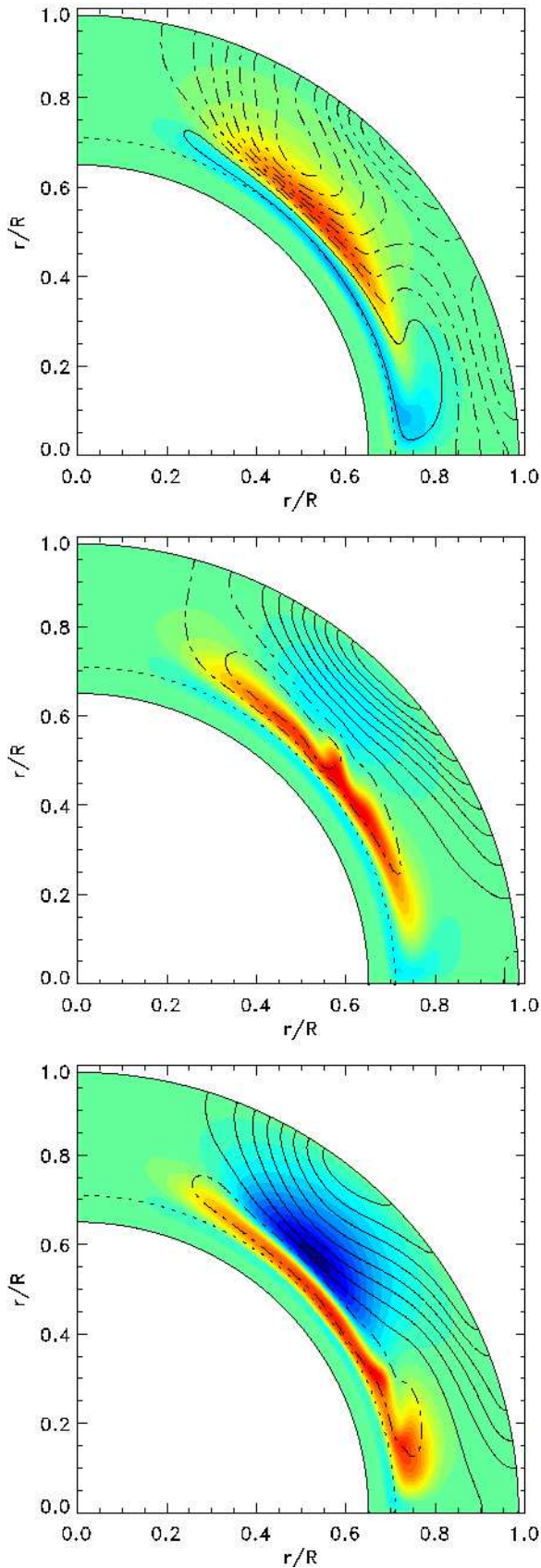


FIG. 5.— Time evolution of magnetic field (color shades: toroidal field, contour lines: poloidal field lines). The frames shown correspond to $t = 0$, $t = 3.25$, and $t = 6.5$ in Figure 4. The bottom panels shows clearly the breakup of the magnetic layer caused by magnetic buoyancy.

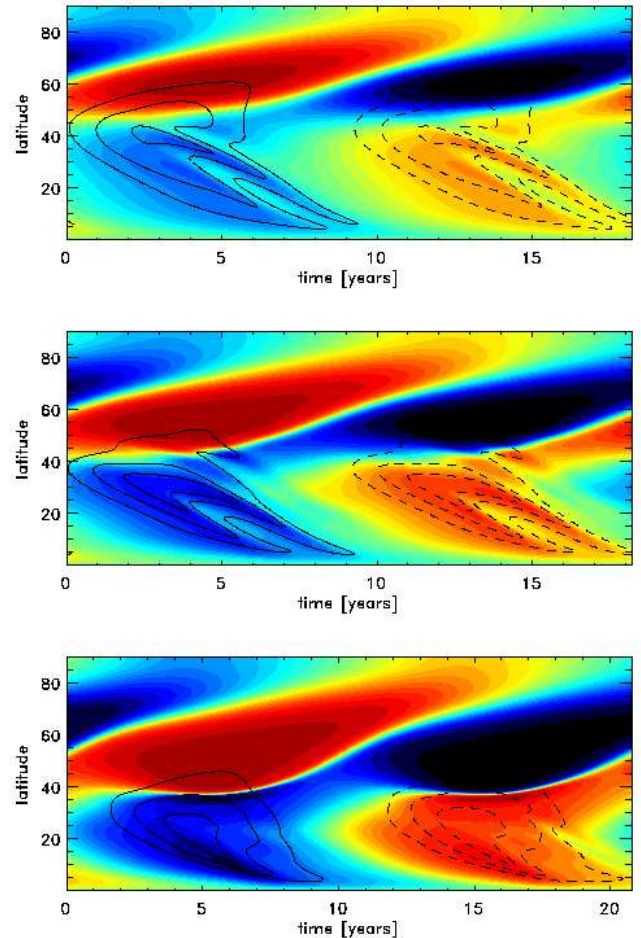


FIG. 6.— Butterfly diagram (contour lines) and radial field at $r = 0.985 R_{\odot}$ (color shades) for the solutions with $\alpha_0 = 0.125 \text{ m s}^{-1}$ (top), 0.25 m s^{-1} (middle), and 0.5 m s^{-1} (bottom). The increase in Lorentz force feedback leads to a confinement of magnetic activity to lower latitudes.

field strength, but does not influence the shape of the solution in great detail (with increased quenching the average profile of α changes, which has a slight influence of the solution). In our model the toroidal field shows only minor changes (1.2, 1.4, and 1.2 T for the cases with α_0 values of 0.125, 0.25, and 0.5 m s^{-1} , respectively), however the profile of the solution changes significantly through the changes in meridional flow and differential rotation. On average stronger feedback leads to a concentration of magnetic activity to lower latitudes, which is the consequence of a strong cycle variability of the meridional flow. While the average flow is roughly the same in all cases, the meridional flow tends to be more concentrated toward the equator during the phase of the cycle when the poloidal field is transported downward, leading to the production of toroidal field at lower latitudes, too. Even though interesting, this feature has most likely no relevance to solar dynamos, since the degree of feedback required is not observed (e.g. torsional oscillations with an amplitude of around 20 nHz). When considering solutions with such a large degree of feedback magnetic buoyancy also plays an important role (subsection 3.4).

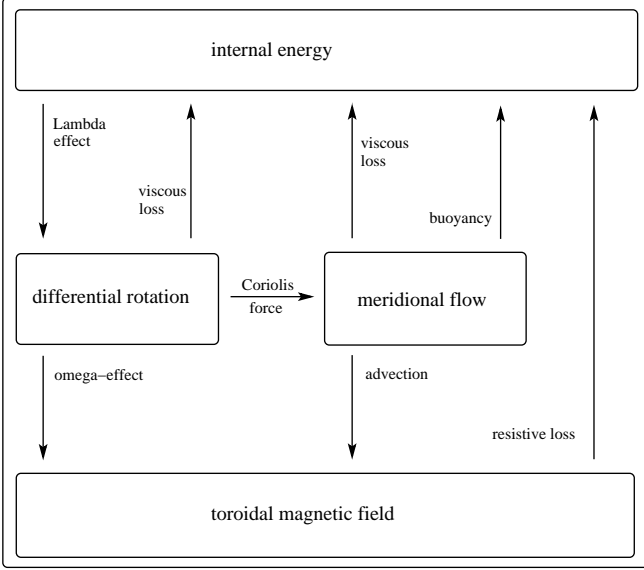


FIG. 7.— Schematic view of energy fluxes in the coupled dynamo-differential rotation model.

3.2. Energy flows within model

In this section we discuss the dynamo solutions by analyzing the energy flows between the different energy reservoirs of the model. This allows us to understand the saturation mechanism of the non-linear dynamo on a more quantitative level.

Figure 7 shows a schematic of the energy flows in our coupled dynamo-differential rotation model. For reasons of simplicity we consider here only the energy of the toroidal field, since the energy of the poloidal field plays only a minor role. The following equations describe the change of rotation energy E_Ω , energy of meridional flow E_M , and energy of toroidal magnetic field E_B :

$$\frac{\partial E_\Omega}{\partial t} = Q_\Lambda - Q_\nu^\Omega - Q_C - Q_L^\Omega \quad (20)$$

$$\frac{\partial E_M}{\partial t} = Q_C - Q_\nu^M - Q_B - Q_L^M \quad (21)$$

$$\frac{\partial E_B}{\partial t} = Q_L^\Omega + Q_L^M - Q_\eta, \quad (22)$$

where the energy reservoirs are given by

$$E_\Omega = \int dV \frac{1}{2} \varrho_0 s^2 \Omega^2 \quad (23)$$

$$E_M = \int dV \varrho_0 \frac{\mathbf{v}_m^2}{2} \quad (24)$$

$$E_B = \int dV \frac{B_\Phi^2}{2\mu_0} \quad (25)$$

and the exchange terms are given by

$$Q_\Lambda = - \int dV \nu_t \varrho_0 s \left(\frac{\partial \Omega}{\partial r} \Lambda_{r\phi} + \frac{1}{r} \frac{\partial \Omega}{\partial \theta} \Lambda_{\theta\phi} \right) \quad (26)$$

$$Q_\nu^\Omega = \int dV \nu_t \varrho_0 s^2 \left[\left(\frac{\partial \Omega}{\partial r} \right)^2 + \left(\frac{1}{r} \frac{\partial \Omega}{\partial \theta} \right)^2 \right] \quad (27)$$

$$Q_C = - \int dV s^2 \varrho_0 \mathbf{v}_m \cdot \nabla \frac{\Omega^2}{2} \quad (28)$$

$$Q_L^\Omega = - \int dV \Omega \mathbf{B}_p \cdot \nabla (s B_\Phi) \quad (29)$$

$$Q_\nu^M = \int dV \frac{1}{2} [R_{rr} E_{rr} + 2R_{r\theta} E_{r\theta} + R_{\theta\theta} E_{\theta\theta} + R_{\phi\phi} E_{\phi\phi}] \quad (30)$$

$$Q_B = - \int dV v_r \varrho_0 g \frac{s_1}{\gamma} \quad (31)$$

$$Q_L^M = \int dV \frac{B_\Phi}{s} \mathbf{v}_m \cdot \nabla (s B_\Phi) \quad (32)$$

$$Q_\eta = \int dV \frac{\eta_t}{s^2} \left[\left(\frac{\partial (s B_\Phi)}{\partial r} \right)^2 + \left(\frac{1}{r} \frac{\partial (s B_\Phi)}{\partial \theta} \right)^2 \right] \quad (33)$$

Here $s = r \sin \theta$ denotes the distance to the axis of rotation and

$$\int dV = 4\pi \int_{r_{\min}}^{r_{\max}} dr \int_0^{\pi/2} d\theta r^2 \sin \theta \quad (34)$$

denotes the integral over the entire volume of the sphere from $r = r_{\min}$ to $r = r_{\max}$. We emphasize that we solve our model only for the northern hemisphere but we compute from that the energy conversion for the entire sphere. The quantity $\mathbf{v}_m = (v_r, v_\theta, 0)$ denotes the meridional flow and $\mathbf{B}_p = (B_r, B_\theta, 0)$ the poloidal magnetic field.

Rempel (2005a) showed already the derivation for the non-magnetic part of the system Eqs. (20) - (22). The exchange terms Eqs. (26) - (33) are not unique expressions since they can be transformed in the form:

$$expression_1 = \nabla \cdot \mathbf{flux} + expression_2, \quad (35)$$

provided that the volume integral over the flux divergence vanishes. We use the appropriate closed boundary conditions for all variables except for B_Φ , however, the resistive flux across the upper boundary turns out to be negligible. We also emphasize that we defined a few of the exchange terms with an opposite sign than in Rempel (2005a). Here all Q_{\dots} are positive so that the signs in Eqs. (20) - (22) clearly state which terms are sources and which are sinks for the corresponding energy reservoir.

The third column of table 1 summarizes the energy flow of the differential rotation reference model we use for all dynamo simulations. In this model the Λ -effect converts 1.4% of the solar energy flux into rotation energy. 57.4% of this energy is lost directly through viscous dissipation of the differential rotation, while 42.5% is flowing into the reservoir of meridional flow by means of the Coriolis force. The major fraction of this amount returns into the reservoir of internal energy through work against buoyancy force, only a small fraction $< 1\%$ through viscous dissipation of the meridional flow. In the reference model the pole-equator difference in rotation rate is 27% of the core rotation rate.

Columns 4 to 10 of table 1 summarize the results obtained from the dynamo models with different α and η_{cz} values. The top portion of Table 1 shows the pole-equator difference in rotation rate, the amplitude of torsional oscillations, the maximum toroidal and radial field strength, average magnetic energy and fluctuation of magnetic energy over a dynamo cycle as well as maximum magnetic energy and flux of one polarity at the

TABLE 1
SUMMARY OF RESULTS

quantity	unit	reference	$\alpha_0 = 0.125 \text{ m s}^{-1}$	$\alpha_0 = 0.25 \text{ m s}^{-1}$	$\alpha_0 = 0.5 \text{ m s}^{-1}$	$\eta_{cz} = 5 \times 10^7 \text{ m}^2 \text{ s}^{-1}$			
$(\bar{\Omega}_{\text{eq}} - \bar{\Omega}_{\text{pole}}) / \Omega_0$		0.27	0.21	(0.21)	0.15	(0.15)	0.1	(0.12)	0.15
$\max(\Omega - \bar{\Omega})_{90^\circ}$	[nHz]	...	4.7	(5.8)	11.5	(11.1)	17.7	(24.2)	12.9
$\max(\Omega - \bar{\Omega})_{60^\circ}$	[nHz]	...	3.5	(2.9)	6.9	(5.8)	8.3	(12.1)	9.7
$\max(B_\Phi)$	[T]	...	1.2	(1.2)	1.4	(1.1)	1.2	(1.2)	1.5
$\max(B_r)$	[T]	...	0.014	(0.015)	0.022	(0.021)	0.027	(0.047)	0.02
\bar{E}_B	$[10^{31} \text{ J}]$...	2.8	(3.5)	4.6	(4.4)	5.1	(4.6)	4.9
$\max[(E_B - \bar{E}_B) / \bar{E}_B]$...	0.12	(0.15)	0.22	(0.26)	0.26	(0.55)	0.21
$\max(E_B^+)_{\text{bc}}$	$[10^{31} \text{ J}]$...	1.7	(2.1)	2.2	(2.2)	2.1	(2.7)	2.4
$\max(\Phi^+)_{\text{bc}}$	$[10^{16} \text{ Wb}]$...	1.1	(1.3)	1.2	(1.3)	1.2	(1.6)	1.2
Q_Λ	$[F_\odot]$	0.014	0.013	(0.013)	0.011	(0.01)	0.008	(0.008)	0.012
Q_ν^Ω	$[Q_\Lambda]$	0.574	0.5	(0.484)	0.405	(0.415)	0.304	(0.357)	0.459
Q_C	$[Q_\Lambda]$	0.425	0.43	(0.429)	0.445	(0.423)	0.465	(0.412)	0.441
Q_L^Ω	$[Q_\Lambda]$...	0.069	(0.087)	0.149	(0.162)	0.232	(0.231)	0.1
Q_B	$[Q_\Lambda]$	0.419	0.41	(0.404)	0.414	(0.384)	0.423	(0.357)	0.409
Q_ν^M	$[Q_\Lambda]$	0.005	0.005	(0.005)	0.007	(0.007)	0.01	(0.01)	0.008
Q_L^M	$[Q_\Lambda]$...	0.014	(0.019)	0.024	(0.032)	0.033	(0.043)	0.023
Q_η	$[Q_\Lambda]$...	0.083	(0.104)	0.172	(0.192)	0.268	(0.272)	0.123
Q_η	$[F_\odot]$...	0.0011	(0.0014)	0.0019	(0.0019)	0.0021	(0.0022)	0.0015

NOTE. — Summary of dynamo simulations discussed. The top portion shows a few global properties of the solution, the bottom portion the energy transfer terms defined by Eqs. (26) - (33). Values in brackets refer to models in which the magnetic buoyancy term is switched off (see subsection 3.4 for further details). The maximum of $\Omega - \bar{\Omega}$ and B_r is evaluated at $0.985 R_\odot$, the maximum of B_Φ at $0.735 R_\odot$. $\max(E_B^+)_{\text{bc}}$ and $\max(\Phi^+)_{\text{bc}}$ are the maximum values of magnetic energy and magnetic flux integrated over the interval $[0.71, 0.76] R_\odot$, considering only one toroidal field polarity. The value of Q_Λ and Q_η (last row) are given relative to the solar luminosity, all the other energy exchange terms are relative to Q_Λ . Note that the accuracy of the energy exchange terms is around 0.001, so the equilibrium relations $Q_\Lambda = Q_\nu^\Omega + Q_C + Q_L^\Omega$, $Q_C = Q_\nu^M + Q_B + Q_L^M$, and $Q_\eta = Q_L^\Omega + Q_L^M$ are only fulfilled within that error margin.

base of the convection zone. The bottom portion shows the energy exchange terms Eqs. (26) to (33) averaged over a cycle (12 cycles in case of the irregular solutions shown in Fig. 8). The quantity Q_Λ is given in units of the solar energy flux and the following terms relative to Q_Λ . The last line gives Q_η in units of the solar energy flux.

As already mentioned in the previous section, increasing the value of α does not lead to a significant increase of the toroidal field strength. The same applies to the magnetic energy and the magnetic flux at the base of the convection zone. At the same time the equator-pole difference of the differential rotation decreases monotonically from $0.21\Omega_0$ in the case with $\alpha_0 = 0.125 \text{ m s}^{-1}$ to $0.1\Omega_0$ in the case with $\alpha_0 = 0.5 \text{ m s}^{-1}$. For comparison, the reference model has an equator-pole difference of $0.27\Omega_0$. This shows clearly that the saturation mechanism of the dynamo is the reduction of the shear through Lorentz force feedback on differential rotation. This becomes also evident by looking at the energy exchange terms Q_ν^Ω and Q_L^Ω : While Q_ν^Ω is decreasing and Q_L^Ω increasing, the sum of both relative to Q_Λ remains roughly the same, meaning that in the dynamo solutions viscous stress is replaced by Maxwell stress. The energy transfer to meridional flow Q_C shows only a weak increase with α_0 . The energy transferred in total into magnetic energy (and dissipated back to internal energy), Q_η increases relative to Q_Λ from 8.3% to 26.1% with increasing α_0 .

Even though we use a fixed parameterization for the Λ -effect in our model, the energy which is converted by the Λ -effect (Q_Λ) decreases with increasing α_0 , since in Eq. (26) also the shear enters. As a consequence, Q_η does not change that much in absolute units (last row in Table 1) when α_0 is increased from 0.25 m s^{-1} to 0.5 m s^{-1} . This is consistent with the almost constant value of the magnetic energy in both cases.

A different way to look at the saturation is as follows. In the model with $\alpha_0 = 0.5 \text{ m s}^{-1}$ the radial surface field (a measure for the poloidal field strength) almost doubled compared to the model with $\alpha_0 = 0.125 \text{ m s}^{-1}$. At the same time equator-pole difference of Ω is reduced to roughly half the value, leading to the same toroidal field strength through the Ω -effect. Since the Lorentz force is proportional to the product of poloidal and toroidal field, the feedback on Ω has almost doubled. This leaves however the question if it is possible to obtain larger toroidal field strength by going in the opposite direction and reducing the poloidal field strength. Inspecting Eq. (6) gives and estimate of the toroidal/poloidal field ratio, which can be obtained through the Ω -effect:

$$\frac{B_\Phi}{B_\theta} \sim \tau \frac{\partial \Omega}{\partial \theta} \sim 100, \quad (36)$$

where we used $\tau = 5 \text{ years}$ and $\partial \Omega / \partial \theta \sim 0.2 \Omega_0$. For the model with $\alpha_0 = 0.125 \text{ m s}^{-1}$ B_θ within the convection zone peaks at around 0.03 T , which does not allow

for much larger toroidal field keeping in mind the reduction of the poloidal field in this thought experiment and considering that the estimate Eq. (36) does not include resistive loss during the amplification phase.

The cycle variation of Ω (torsional oscillation) increases roughly proportional to α_0 from around 4.7 nHz to 18 nHz at the pole, the change at 60° latitude is about half that value. Given the observational constraint that solar torsional oscillations at 60° have an amplitude of around 2 nHz, the solar dynamo is most likely operating in a regime with weak Lorentz force feedback, close to our model with $\alpha_0 = 0.125 \text{ m s}^{-1}$ or even smaller. In that model the amount of energy converted to magnetic energy is around 8% of the energy converted into differential rotation by the Λ -effect, in absolute units, around 0.1% of the solar energy flux. This number is interestingly very close to the variation of solar irradiance throughout the solar cycle.

In the last column of Table 1 we show results obtained from a model with $\alpha_0 = 0.125 \text{ m s}^{-1}$, but magnetic diffusivity of only $5 \times 10^7 \text{ m}^2 \text{ s}^{-1}$ in the convection zone. This model is very close to the model with $\alpha_0 = 0.25 \text{ m s}^{-1}$ and a diffusivity of $10^8 \text{ m}^2 \text{ s}^{-1}$. The magnetic field strength as well as magnetic energy is slightly higher, at the same time the amount of energy extracted from differential rotation is lower due to the lower magnetic diffusivity. Nevertheless, the amplitude of torsional oscillations is larger compared to the model with higher diffusivity.

3.3. Saturation field strength of dynamo

Various models of rising magnetic flux-tubes (Choudhuri & Gilman 1987; Fan et al. 1993; Schüssler et al. 1994; Caligari et al. 1995, 1998) inferred a field strength of around 10 T at the base of the convection zone, which is almost one magnitude more than the field strength we obtain in our model. Since our model is a mean field model, the mean field strength is not necessarily identical to the field strength of individual flux elements in case of an intermittent field. When we compare our mean field solution to a solution with an intermittent field it is required to compare energy densities (which also ensure the same Lorentz force densities) rather than average field strength, since this ensures the same level of dynamic feedback. Suppose an intermittent field with a filling factor f and individual flux elements with field strength B_f . Conserving the mean energy leads a relation between mean field strength B and B_f of $B_f \sim B/\sqrt{f}$. For a filling factor of $f = 0.1$ this would allow for around 4 T for individual flux elements. Another way to estimate maximum field strength is using the field energy directly. If we assume that the toroidal magnetic field is stored at the base of the convection zone close to the equator in a layer with a thickness Δr and a latitudinal extent Δl , the magnetic energy is $E_B \sim 2\pi r \Delta r \Delta l B^2 / (2\mu_0) = \pi r \Phi B / \mu_0$, with the magnetic flux Φ . Observations lead to an estimate of the magnetic flux of $10^{16} - 10^{17} \text{ Wb} = 10^{24} - 10^{25} \text{ Mx}$ (Galloway & Weiss 1981; Schrijver & Harvey 1994); however, the magnetic flux produced during a cycle at the base of the convection zone is not necessarily identical to the observed surface flux. On the one hand a rising flux rope could produce more than one spot group (which would allow for less flux at the base of the

convection zone) on the other hand it is also likely that only a fraction of the flux at the base of the convection zone shows up in spots at the surface. The flux value we mention in Table 1 is the maximum flux of the dominant polarity available at a given time, while the estimates from observations are the cumulative values of flux integrated over the cycle.

If we use the average energy conversion rate of $0.001 F_\odot$ and integrate that over a cycle length of 11 years we end up with an upper (very optimistic) estimate of $1.3 \times 10^{32} \text{ J}$, not considering any dissipative loss. In this case a value of $\Phi = 10^{16} \text{ Wb}$ would allow for $B = 10 \text{ T}$, the higher value of $\Phi = 10^{17} \text{ Wb}$ for only $B = 1 \text{ T}$. Accounting for the additional dissipative loss, a field strength of more than a few T seems unlikely unless the average energy conversion rate would be larger. In our model that would lead to a contradiction with the observed amplitude of torsional oscillations.

It has been pointed out by Rempel & Schüssler (2001) that also potential energy of the superadiabatic convection zone can be used for the amplification of magnetic field. In contrast to the amplification through the Ω -effect (shearing up of poloidal field by differential rotation), this does not lead to a feedback on differential rotation. Recently Y. Fan (2006, private communication) repeated simulations of rising flux tubes using an anelastic 3D MHD code. These simulations are therefore not bound to the thin flux tube approximation previously used. Preliminary results show that the low latitude emergence and the observed asymmetries between leading and following spots (the tilt angle is a more complicated problem due to the influence of Coriolis force and twist of the flux tube, which is currently being investigated) can be reproduced with magnetic flux tubes having an initial field strength only around 3 T, which would therefore relax the constraint on the field strength at the base of the convection zone.

3.4. Role of magnetic buoyancy

Our model includes magnetic buoyancy in two different ways: implicit buoyancy as part of the parametrized Babcock-Leighton α -effect and explicit (resolved) buoyancy resulting from solving the full momentum equation. While the first effect is essential for the dynamo model, the latter leads mainly to a distortion of the toroidal magnetic field shown in Figs. 4 to 6 and is not essential for the operation of the model. Having parametrized and resolved buoyancy together in a mean field model is of certain conceptual concern since it washes out the boundary between resolved and parametrized processes. Another point of concern is the fact that most buoyancy instabilities are non-axisymmetric and therefore our axisymmetric model does not capture the most unstable modes. One way of evaluating the importance of the explicit buoyancy in this model is to neglect the term $\sim p_{\text{mag}}$ in Eq. (2) that is responsible for it. This is equivalent to adding to s_1 a perturbation of $-p_{\text{mag}}/p_0$, which means physically that the toroidal field is stored in a buoyancy free equilibrium at the base of the convection zone. The Babcock-Leighton α -effect addresses buoyancy instabilities below the resolved scale and is therefore not in contradiction with this assumption. Since this additional entropy perturbation is not considered in Eq. (5) this leads to a small inconsistency in the entropy

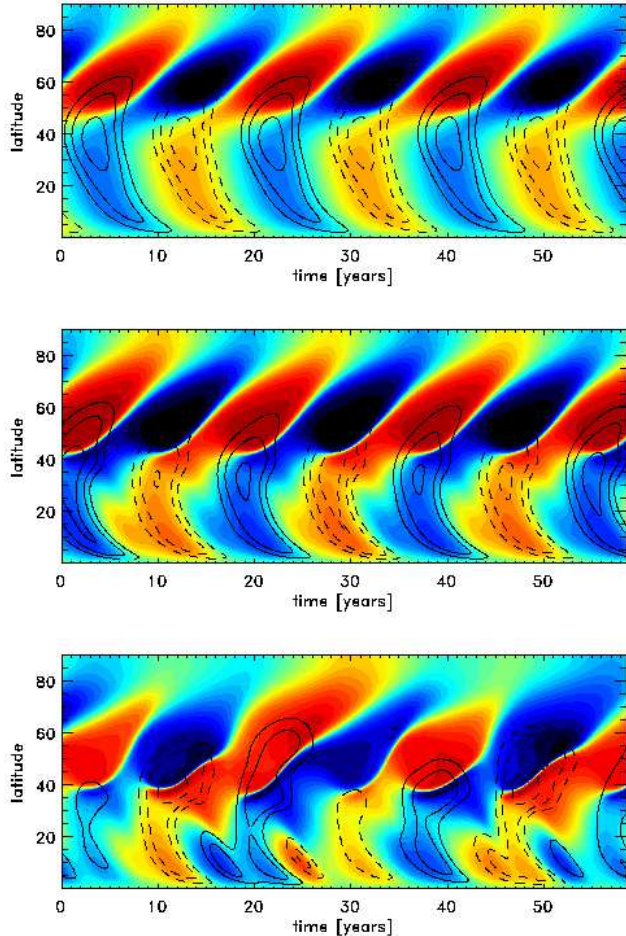


FIG. 8.— Magnetic field evolution for models with magnetic buoyancy switched off. Similar to Fig. 6 solutions with $\alpha_0 = 0.125 \text{ m s}^{-1}$ (top), 0.25 m s^{-1} (middle), and 0.5 m s^{-1} (bottom) are shown.

equation. For the analysis of the energy fluxes we use instead of Eq. (31)

$$Q_B = - \int dV v_r \varrho_0 g \frac{1}{\gamma} \left(s_1 - \frac{p_{\text{mag}}}{p_0} \right). \quad (37)$$

Fig. 8 shows the magnetic field evolution similar to Fig. (6) with magnetic buoyancy switched off. While the top panel (solution with $\alpha_0 = 0.125 \text{ m s}^{-1}$) is very close to the kinematic reference solution with α -quenching, the middle and bottom panels show dynamo solutions with irregular cycles due to the non-linear feedback. Despite the significant difference in the magnetic field pattern and temporal evolution, the differences in the energy exchange terms are not that significant. The most obvious differences occur in the model with $\alpha_0 = 0.5 \text{ m s}^{-1}$ in terms of amplitude of torsional oscillations, radial surface field strength, and variability of magnetic energy. The almost a factor of 2 larger radial field is also the reason for the large irregularity of the solution. The stronger poloidal field at the surface leads through the Lorentz force to a stronger variation in the meridional flow that changes the latitude at which the magnetic field is transported downward. This in return changes the latitudinal extent and strength of the next cycle in a way that a

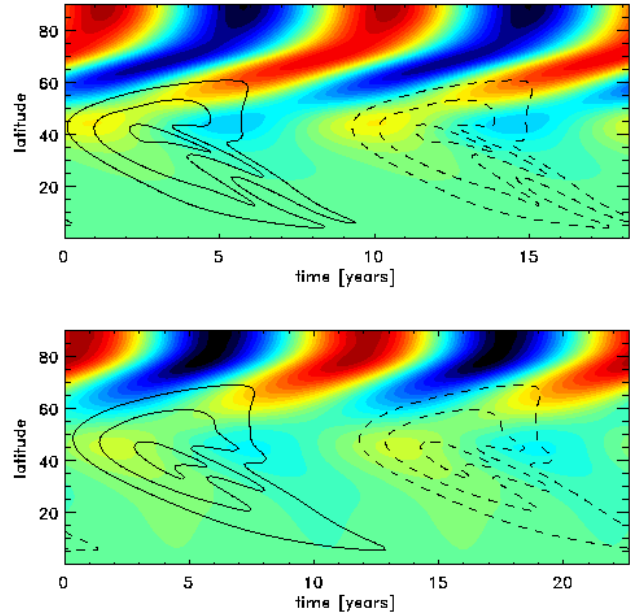


FIG. 9.— Influence of meridional flow profile on phase relation between high latitude torsional oscillation and low latitude toroidal magnetic field. Top: solution shown in Fig. 4 (bottom panel) for reference; bottom: model with meridional flow returning in higher latitudes ($n=2$ instead of $n=3$ in reference model).

periodic solution is not possible anymore. If buoyancy is considered the radial surface field does not reach the threshold required for a highly irregular solution.

4. TORSIONAL OSCILLATIONS

Solar torsional oscillations have been known to exist for more than two decades. Howard & Labonte (1980) presented the first observations of torsional oscillations using Mt. Wilson Doppler measurements and pointed out the 11 year periodicity and the relation to the solar cycle. These early observations showed only the equatorward propagating branch at low latitudes. The high latitude branch (above 60°), which is in amplitude at least twice as strong as the equatorward propagating branch, was found more recently through helioseismic measurements by Toomre et al. (2000); Howe et al. (2000); Antia & Basu (2001); Vorontsov et al. (2002); Howe et al. (2005). These inversions also show that the high latitude signal penetrates almost all the way to the base of the convection zone. The depth penetration of the low latitude signal is more uncertain due to the lower amplitude that is comparable to the uncertainties of the inversion methods in the lower half of the convection zone.

4.1. Mechanical forcing of torsional oscillations

The models discussed so far can only explain the polar branch of the torsional oscillation pattern as a very robust result through the feedback of mean field Lorentz force on differential rotation (mechanical forcing). We also showed that some dynamo models lead to quite significant amplitudes of these oscillations, contrary to observation, which therefore impose constraints on dynamo parameters (amplitude of α -effect and the magnetic diffusivity in convection zone). Other information that can

be extracted from torsional oscillations is their phase relative to the magnetic cycle. The phase relation shown in Fig. 3 of Vorontsov et al. (2002) is such that the pole is rotating faster during solar minimum and slower during maximum, when solar activity peaks around 15° latitude. In order to determine the phase relation in our model, we have to define what phase corresponds to 'solar minimum' and 'solar maximum', given a butterfly diagram which is close to, but not exactly, solar like. If we define 'solar maximum' through the maximum field strength at the base of the convection zone, the location of the activity belt is at around 40° and the torsional oscillation pattern changes from faster to slower rotation at the pole during that time. If we however define 'solar maximum' as the time where the activity belt is around 15° latitude, the phase relation of the model matches the observed torsional oscillations. Since the phase in a flux-transport dynamo is a consequence of the advection of field by the meridional flow, while the amplitude depends on details of microphysics that might not be well represented or even missing in this mean field model (e.g. a tachocline α -effect), the latter definition is most likely more robust and should be used when comparing results to the sun. The phase relation is indeed tied to the structure of the meridional flow. Fig. 9 compares the model shown in Fig. 4 with model that has a meridional flow returning at higher latitudes (we used instead of $n = 3$ and $\Lambda_0 = 1$ $n = 2$ and $\Lambda_0 = 0.8$ in the reference model). While in the original model slower rotation at the pole coincided with an activity belt location at around 20° , it coincides with an activity belt location at around 30° in the latter model. Also note that the dynamo period of the latter model is around 22.5 years instead of 18 years, due to the longer overturning time of the meridional flow.

4.2. Thermal forcing of torsional oscillations

An alternative explanation for the low latitude branch of the torsional oscillations was given by Spruit (2003): Enhanced surface cooling in the active region belt leads to a pressure imbalance that drives a geostrophic flow at the edges of the active region belt showing the properties of the observed pattern. The low latitude oscillation pattern would be therefore purely surface driven and not a signature of Lorentz force feedback within the convection zone.

We can include the idea of Spruit in our model by parameterizing a surface cooling term that depends on the toroidal field at the base of the convection zone. To this end we change the upper boundary condition such that the entropy gradient corresponds to an increase in energy flux. With the diffusive convective energy flux $\mathbf{F}_c = \kappa_t \varrho_0 T_0 c_v \nabla s_1$ and $c_v = (\gamma - 1)^{-1} p_0 / (\varrho_0 T_0)$ this leads to

$$\frac{\partial s_1}{\partial r} = -\frac{\gamma - 1}{\kappa_t p_0} \epsilon F_\odot \left(\frac{(\sin \theta)^2 \bar{B}_{\Phi, bc}}{B_{\text{ref}}} \right)^2. \quad (38)$$

Here $\bar{B}_{\Phi, bc}(\theta)$ is the toroidal field averaged according to Eq. (19) between $0.71 R_\odot$ and $0.76 R_\odot$, which is also used for the Babcock-Leighton α -effect. B_{ref} is a reference field strength used for normalization, ϵ determines the amplitude of the flux enhancement as fraction of the solar luminosity. In order to illustrate this effect and allow a comparison to the observed solar torsional oscillation

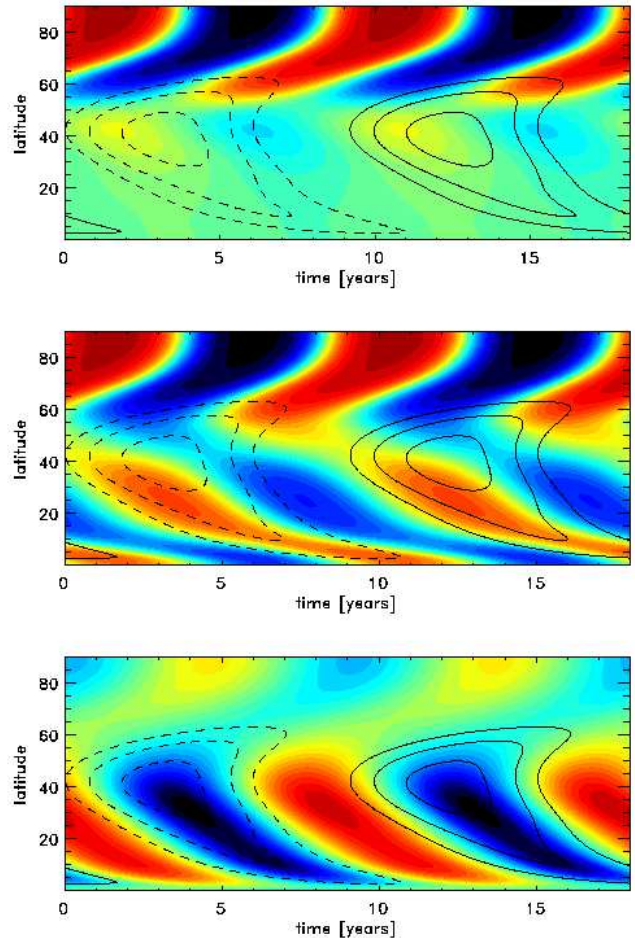


FIG. 10.— Torsional oscillations caused through enhanced radiative losses in the active region belt. Top: reference model with no surface cooling; middle: model with surface cooling, the maximum amplitude is $4n\text{Hz}$, bottom: surface temperature variation, the maximum amplitude is 0.2 K.

we introduce a factor $(\sin \theta)^2$ in front of \bar{B}_Φ to correct the latitudinal field strength profile of the butterfly diagram accordingly (this is consistent with the $(\sin \theta)^2$ factor introduced in the α -effect for the same reason). We use a dynamo model with magnetic buoyancy switched off and a smaller value of α (0.1 ms^{-1}) than before in order to obtain an amplitude of the torsional oscillations close to the observed one (around 4 nHz at the pole and 2 nHz at 60° latitude). Fig. 10 (top panel) shows the torsional oscillation and butterfly diagram for the dynamo solution not considering the surface cooling. The middle panel shows the solution with surface cooling considered using the parameters $\epsilon = 2 \times 10^{-2}$ and $B_{\text{ref}} = 1 \text{ T}$. The cooling of the active region belt drives a equatorward propagating torsional oscillation with an amplitude of around 1.5 nHz, with the peak values at the edges of the active region belt. The amplitude of the associated temperature perturbations (shown in the bottom panel) is around 0.2 K. The peak cooling rate in our model is close to 0.75% of the solar energy flux, the surface intergrated luminosity variation corresponds to around 0.23% luminosity change throughout the cycle, about a factor of 3 larger than the observed one. We emphasize that this value is imposed

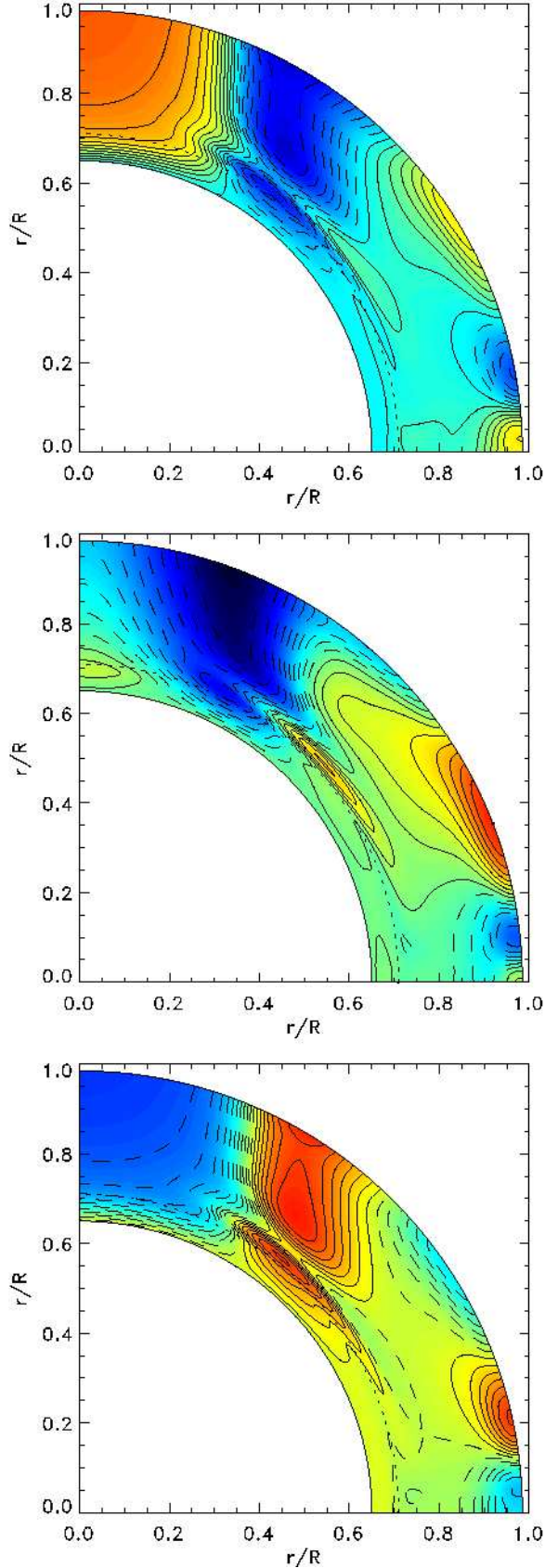


FIG. 11. — Torsional oscillations for model with additional surface cooling. The frames (top to bottom) correspond to the times $t = 1$, $t = 3.5$, and $t = 6$, in Fig. 11. While the polar branch of the torsional oscillations penetrates all the way to the base of the convection zone, the equatorial branch caused by surface cooling is confined close to the surface.

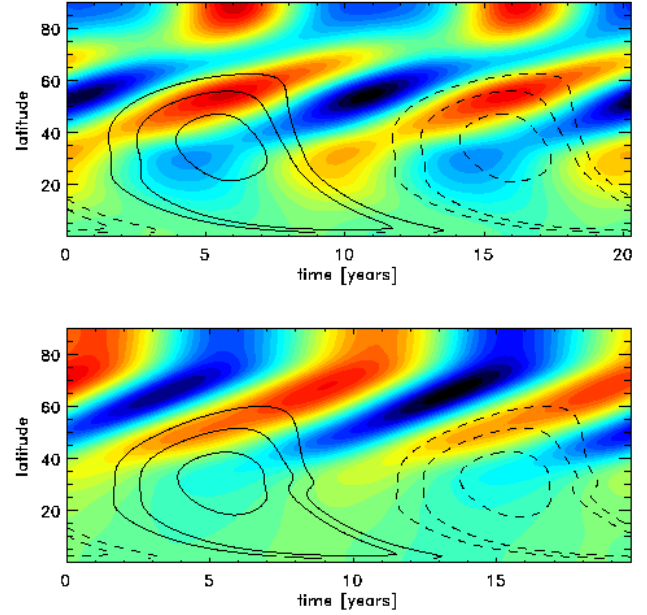


FIG. 12. — Top: near surface torsional oscillation caused through quenching of turbulent viscosity, the maximum amplitude is 0.77 nHz; bottom: torsional oscillation caused through quenching of turbulent viscosity and heat conductivity, the maximum amplitude is 3.1 nHz, respectively.

at $r = 0.985 R_{\odot}$ and does not necessarily resemble the value required in a more realistic model extending all the way into the photosphere and using a more sophisticated description of convection than the diffusion approximation. Fig. 11 shows three snapshots of the evolution of the torsional oscillation in a r - θ -plane. While the poleward propagating branch (driven by Lorentz force feedback on differential rotation) is penetrating all the way down to the base of the convection zone, the equatorward propagating branch (driven through the surface cooling) is more concentrated toward the surface. As a side effect of the surface cooling the model also shows close to the surface an inflow into the active region belt with a peak amplitude of around 5 m s^{-1} . This value is in agreement with the theory of Spruit (2003), where the meridional component is a consequence of an Ekman boundary layer at the solar surface. Komm et al. (1993); Komm (1994) derived an average inflow into the active region belt of around 5 m s^{-1} from Kitt Peak magnetograms. More recently also helioseismology showed a mean inflow into the active region belt with an amplitude from 2 m s^{-1} to 8 m s^{-1} (Zhao & Kosovichev 2004).

4.3. Forcing of torsional oscillations through quenching of viscosity and heat conductivity

So far we only considered the 'macroscopic' Lorentz force feedback in terms of the Lorentz force computed from the magnetic mean field. Alternatively we can consider 'microscopic' feedback through quenching of turbulent motions. This type of feedback is typically used in kinematic models in terms of α -quenching to saturate the dynamo. We consider here the quenching of turbulent viscosity and heat conductivity. Since in our model the turbulent viscosity scales the amplitude of the Λ -

effect, quenching of ν_t reduces the energy input into the system and leads to a saturation of the dynamo as consequence of a reduction in differential rotation similar to the 'macroscopic' feedback discussed above. Additional quenching of turbulent heat conductivity leads to changes in entropy profile of the convection zone. Since the differential rotation is close to a baroclinic balance, a change in the entropy profile also forces changes in the differential rotation. Fig. 10 (top panel) shows torsional oscillations and the butterfly diagram obtained from a dynamo model with $\alpha_0 = 0.125 \text{ ms}^{-1}$ and ν_t quenching with $B_{\text{eq}} = 1 \text{ T}$ according to Eq. (10). Fig. 12 (bottom panel) shows torsional oscillations resulting from additional quenching of the turbulent heat conductivity. Note the different phase relation of the torsional oscillations with respect to the magnetic butterfly diagram compared to the results with 'macroscopic' Lorentz force feedback. Quenching of turbulent heat conductivity alone is not a process that can efficiently saturate the dynamo, since it leads more to a modulation of Ω rather than a reduction in the equator-pole difference. It can however significantly change the torsional oscillation pattern. Since there are additional effects such as anisotropic heat transport, which are not considered in our model, we emphasize here only the interesting result that the amplitude of these thermally forced oscillations is quite significant. Quenching of turbulent viscosity is along the lines of Λ -quenching considered before by Kitchatinov & Pipin (1998); Kitchatinov et al. (1999); Küker et al. (1999).

5. PARAMETER DEPENDENCE

The results presented in this paper were obtained using a mean field model that requires parameterizations of unresolved processes. Therefore it is necessary to test to which extent results are sensitive with respect to details of the parameterizations used. Our differential rotation / meridional flow model has three important parameters: n describing the profile of the Λ -effect in latitude, Λ_0 determining the amplitude of the Λ -effect, and the turbulent diffusivities ν_t , κ_t (both have same value in our model). Λ_0 has been chosen to get differential rotation with the correct amplitude. For a fixed value of Λ_0 , ν_t and κ_t determine the amplitude of the meridional flow. The latter has been chosen to lead to dynamo simulations with a period close to 22 years. The parameter n determines the extent of the meridional flow cell in latitude. Reasonable choices are in the range 2–4 (for values above 4 differential rotation is confined to low latitudes, which also contradicts observations). Within this range the influence on the solutions is rather limited (see Fig. 9). A fourth parameter not discussed in this paper is the direction of the turbulent angular momentum flux with respect to the axis of rotation. In this paper we used a fixed value of $\lambda = 15^\circ$, as has been used also for most models in Rempel (2005b). Significantly larger values lead to more complicated meridional flow patterns (permanent reverse cell in high latitudes), smaller values require and increase of Λ_0 to maintain the differential rotation amplitude, which in return leads to larger meridional flow speeds, requiring significantly lower values for ν_t and κ_t to obtain a solar-like dynamo period. We computed solutions (not shown in this paper) with the parameters $\lambda = 7.5^\circ$, $\Lambda_0 = 2$ and $\nu_t = \kappa_t = 1.25 \times 10^8 \text{ m}^2 \text{ s}^{-1}$ that show no significant difference, except that the am-

plitude of the torsional oscillations is around 50% larger due to the reduced viscous damping. Therefore calibrating our reference model to be solar-like does not leave a lot of choice for the parameters of the differential rotation model. Using such a calibrated reference model, the following main results are not strongly dependent on the additional dynamo parameters (α -effect, η_t) providing the magnetic diffusivity is low enough to be in an advection dominated regime: The dynamo saturates with a toroidal (mean) field strength of about 1.2 to 1.5 T at the base of the convection zone, the maximum magnetic flux produced during a cycle is around 10^{16} Wb , the energy converted on average into magnetic energy is 0.1% to 0.2% of the solar luminosity (more likely 0.1 incorporating additional constraints set by helioseismic observations of torsional oscillations). Another important result is that the dynamo saturates already through reduction of differential rotation at a field strength where the direct feedback on the meridional flow is insignificant. Therefore the fundamental character of the flux-transport dynamo remains unaltered (the non-linear feedback tends to concentrate magnetic activity even closer toward the equator).

6. IMPLICATIONS FOR SOLAR DYNAMO

In this paper we discussed 'dynamic' flux-transport dynamo by combining a mean field differential rotation model with a mean field dynamo model. The main results from this study are the following

- The non-kinematic Babcock-Leighton flux-transport dynamo saturates through a reduction of the amount of differential rotation at a toroidal field strength of around 1.5 T. This field strength is found to be fairly independent from particular choices of the strength of the α -effect and value of magnetic diffusivity. The energy conversion rate of the dynamo is around $0.001 L_\odot$.
- The Lorentz force feedback (at the saturation field strength of around 1.5 T) on the meridional flow is not strong enough to switch off the equatorward transport of toroidal field required for the operation of the flux-transport dynamo. This is consistent with the findings of Rempel (2006) who studied the modification of meridional flow by an imposed stationary toroidal magnetic field.
- The Lorentz force feedback on differential rotation leads to torsional oscillations that are comparable (in terms of amplitude and phase with respect to the magnetic butterfly) to the high latitude branch of the pattern inferred from helioseismology. The low latitude branch cannot be explained through Lorentz force feedback in our model. A model including thermal forcing through increased radiative losses in the active region belt (Spruit 2003) also produces the low latitude branch. Thermal forcing is found to be very efficient in the sense that temperature variation of only a few tenth of a degree are sufficient to explain the observed amplitudes of torsional oscillations.

The results presented here cannot answer the question of whether the solar dynamo is a flux-transport dynamo or not; however, they make the case stronger for a

flux transport dynamo since they demonstrate that flux-transport dynamos also function in the non-kinematic regime (the meridional flow is strong enough to transport toroidal field of around 1.5 T strength equatorward). Additional to that the torsional oscillations caused by the macroscopic Lorentz force in a flux-transport dynamo are in agreement with helioseismic results (in terms of amplitude and phase relation). With 'in agreement' we mean here that there are no features produced that are not observed; however there are observed features (the low latitude branch) that require additional physics such as thermal forcing (Spruit 2003). The idea of thermal forcing of the low latitude branch is also consistent with a mean inflow into the active region belt of the order of 5 ms^{-1} that has been observed in magnetograms (Komm et al. 1993; Komm 1994) and inferred from helioseismology (Zhao & Kosovichev 2004). We emphasize that thermal forcing is a very efficient process, since only tiny temperature fluctuations of the order of a few tenths of a degree can drive large scale flows with the observed amplitude. This opens the possibility that also other processes such as the magnetic quenching of the convective energy flux in the solar convection zone contribute.

Covas et al. (2000, 2004, 2005) presented a $\alpha\Omega$ -dynamo model (no meridional flow) including a simplified momentum equation for considering feedback on differential rotation. In their simulation they were able to reproduce additional to the polar branch also the low latitude oscillations pattern. The main difference between their and our model is that we use a flux-transport dynamo with a non-local Babcock-Leighton α -effect, while they use a classic $\alpha\Omega$ -dynamo model with a (negative) local α -effect in the convection zone to obtain an equatorward propagating dynamo wave. The requirement to have a propagating dynamo wave leads to a fixed phase relation between poloidal and toroidal field, which automatically leads to a Lorentz force pattern propagating with the field and producing a torsional oscillation pattern associated with the magnetic field. This constraint is relaxed in a flux-transport dynamo, where the propagation of the activity belt is a pure advection effect. Given the fact that the origin of the low latitude oscillation pattern is uncertain and might be entirely surface driven, it is difficult to judge to which extent this discrepancy is of concern for different types of dynamo models and might rule out certain approaches.

We emphasize here that it is essential for models of torsional oscillations to include the full momentum equation, since the Taylor-Proudman constraint applies also to perturbations of Ω ($\partial\Omega_1/\partial z = 0$) and therefore significantly alters the phase relation of the oscillations. Torsional oscillations with $\partial\Omega_1/\partial z \neq 0$ (as observed in the sun at low latitudes) require additional thermal perturbations, which makes also the consideration of an energy

equation essential and favors explanations such as the one proposed by Spruit (2003).

Torsional oscillations contain valuable information about the dynamo processes in the solar interior and are helpful to impose additional constraints on dynamo models. Their interpretation and relation to the dynamo generated magnetic field is complicated since different processes can produce torsional oscillations. As a first step toward using torsional oscillations to probe solar cycle related processes in the solar interior it is important to test the sensitivity of helioseismic inversions to dynamo generated rotation modulations in the solar interior, especially close to the base of the convection zone. This work is currently done by Howe et al. (2004, 2006) for different helioseismic techniques using artificial data and also model results discussed in this paper.

The model presented here sets strong constraints for the strength of toroidal field at the base of the convection zone that can be achieved through the shear by differential rotation. We find in our model a value of around 1.5 T (15 kG) as upper limit. These results are in agreement with recent findings of Gilman & Rempel (2005) who showed that significantly larger field strength would require a very strong mechanism replenishing energy to differential rotation (replenishment time-scale of less than a month). The fairly low field strength (compared to convective equipartition) raises the question of how these fields can rise through the convection zone and form coherent sunspots at the surface. On the one hand recent work by Y. Fan (2006, private communication) suggests that 3D simulations of rising flux tubes can reproduce most sunspot properties starting with field strengths around 2 to 3 T at the base of the convection zone (as opposed to thin flux tube simulations requiring around 10 T); on the other hand recent work by Brummell et al. (2002); Cattaneo et al. (2006) is questioning the existence of coherent buoyant structures. In our model these uncertainties are hidden behind the parameterization of the Babcock-Leighton α -effect. Since the existence of this effect is known from surface observations (it is the essential ingredient in models describing the evolution of the surface magnetic field assimilating real observations (Schrijver et al. 2002; Baumann et al. 2004, 2006; Wang et al. 2005)) this is of secondary concern for the model presented here; it is however of primary interest for understanding the microphysics beyond the mean field approach.

The author thanks M. Dikpati, P. A. Gilman and K. B. MacGregor for very helpful comments on a draft of this paper. Very helpful suggestions by the anonymous referee are also acknowledged.

REFERENCES

- Antia, H. M. & Basu, S. 2001, *ApJ*, 559, L67
 Babcock, H. W. 1961, *ApJ*, 133, 572
 Baumann, I., Schmitt, D., & Schüssler, M. 2006, *A&A*, 446, 307
 Baumann, I., Schmitt, D., Schüssler, M., & Solanki, S. K. 2004, *A&A*, 426, 1075
 Brandenburg, A., Moss, D., Ruediger, G., & Tuominen, I. 1991, *Geophysical and Astrophysical Fluid Dynamics*, 61, 179
 Brandenburg, A., Moss, D., & Tuominen, I. 1992, *A&A*, 265, 328
 Brandenburg, A., Tuominen, I., Moss, D., & Ruediger, G. 1990, *Sol. Phys.*, 128, 243
 Braun, D. C. & Fan, Y. 1998, *ApJ*, 508, L105
 Brummell, N., Cline, K., & Cattaneo, F. 2002, *MNRAS*, 329, L73
 Brun, A. S. & Toomre, J. 2002, *ApJ*, 570, 865
 Caligari, P., Moreno-Inertis, F., & Schüssler, M. 1995, *ApJ*, 441, 886
 Caligari, P., Schüssler, M., & Moreno-Inertis, F. 1998, *ApJ*, 502, 481

- Cattaneo, F., Brummell, N. H., & Cline, K. S. 2006, *MNRAS*, 365, 727
- Choudhuri, A. R. & Gilman, P. A. 1987, *ApJ*, 316, 788
- Choudhuri, A. R., Schüssler, M., & Dikpati, M. 1995, *A&A*, 303, L29
- Covas, E., Moss, D., & Tavakol, R. 2004, *A&A*, 416, 775
- . 2005, *A&A*, 429, 657
- Covas, E., Tavakol, R., Moss, D., & Tworkowski, A. 2000, *A&A*, 360, L21
- Dikpati, M. 2005, *Advances in Space Research*, 35, 322
- Dikpati, M. & Charbonneau, P. 1999, *ApJ*, 518, 508
- Dikpati, M., de Toma, G., & Gilman, P. A. 2006, *Geophys. Res. Lett.*, 33, 5102
- Dikpati, M., de Toma, G., Gilman, P. A., Arge, C. N., & White, O. R. 2004, *ApJ*, 601, 1136
- Dikpati, M. & Gilman, P. A. 2001, *ApJ*, 559, 428
- Durney, B. R. 1995, *Sol. Phys.*, 160, 213
- Fan, Y., Fisher, G. H., & DeLuca, E. E. 1993, *ApJ*, 405, 390
- Galloway, D. J. & Weiss, N. O. 1981, *ApJ*, 243, 945
- Gilman, P. A. & Miller, J. 1986, *ApJS*, 61, 585
- Gilman, P. A. & Rempel, M. 2005, *ApJ*, 630, 615
- Glatzmaier, G. A. & Gilman, P. A. 1982, *ApJ*, 256, 316
- Haber, D. A., Hindman, B. W., Toomre, J., Bogart, R. S., Larsen, R. M., & Hill, F. 2002, *ApJ*, 570, 855
- Howard, R. & Labonte, B. J. 1980, *ApJ*, 239, L33
- Howe, R., Christensen-Dalsgaard, J., Hill, F., Komm, R., Schou, J., & Thompson, M. J. 2005, *ApJ*, 634, 1405
- Howe, R., Komm, R., & Hill, F. 2000, *Sol. Phys.*, 192, 427
- Howe, R., Rempel, M., Christensen-Dalsgaard, J., Hill, F., Komm, R. W., Schou, J., & Thompson, M. J. 2004, in *ESA SP-559: SOHO 14 Helio- and Asteroseismology: Towards a Golden Future*, 468–+
- Howe, R., Rempel, M., Christensen-Dalsgaard, J., Hill, F., Komm, R. M., Larsen, R. W., Schou, J., & Thompson, M. J. 2006, *ApJ*, October issue
- Jennings, R. L. 1993, *Sol. Phys.*, 143, 1
- Küker, M. & Stix, M. 2001, *A&A*, 366, 668
- Kitchatinov, L. L. & Pipin, V. V. 1998, *Astronomy Reports*, 42, 808
- Kitchatinov, L. L., Pipin, V. V., Makarov, V. I., & Tlatov, A. G. 1999, *Sol. Phys.*, 189, 227
- Kitchatinov, L. L. & Rüdiger, G. 1993, *A&A*, 276, 96
- . 1995, *A&A*, 299, 446
- Komm, R. W. 1994, *Sol. Phys.*, 149, 417
- Komm, R. W., Howard, R. F., & Harvey, J. W. 1993, *Sol. Phys.*, 147, 207
- Küker, M., Arlt, R., & Rüdiger, G. 1999, *A&A*, 343, 977
- Küker, M., Rüdiger, G., & Schultz, M. 2001, *A&A*, 374, 301
- Leighton, R. B. 1969, *ApJ*, 156, 1
- Longcope, D. W., McLeish, T. C. B., & Fisher, G. H. 2003, *ApJ*, 599, 661
- Malkus, W. V. R. & Proctor, M. R. E. 1975, *Journal of Fluid Mechanics*, 67, 417
- Miesch, M. S., Elliott, J. R., Toomre, J., Clune, T. L., Glatzmaier, G. A., & Gilman, P. A. 2000, *ApJ*, 532, 593
- Moss, D., Barker, D. M., Brandenburg, A., & Tuominen, I. 1995, *A&A*, 294, 155
- Moss, D. & Brooke, J. 2000, *MNRAS*, 315, 521
- Muhli, P., Brandenburg, A., Moss, D., & Tuominen, I. 1995, *A&A*, 296, 700
- Rempel, M. 2005a, *ApJ*, 631, 1286
- . 2005b, *ApJ*, 622, 1320
- . 2006, *ApJ*, 637, 1135
- Rempel, M. & Schüssler, M. 2001, *ApJ*, 552, L171
- Rüdiger, G., von Rekowski, B., Donahue, R. A., & Baliunas, S. L. 1998, *ApJ*, 494, 691
- Schrijver, C. J., DeRosa, M. L., & Title, A. M. 2002, *ApJ*, 577, 1006
- Schrijver, C. J. & Harvey, K. L. 1994, *Sol. Phys.*, 150, 1
- Schüssler, M. 1979, *A&A*, 72, 348
- Schüssler, M., Caligari, P., Ferriz-Mas, A., & Moreno-Insertis, F. 1994, *A&A*, 281, L69
- Spruit, H. C. 2003, *Sol. Phys.*, 213, 1
- Tobias, S. M. 1996, *A&A*, 307, L21+
- Toomre, J., Christensen-Dalsgaard, J., Howe, R., Larsen, R. M., Schou, J., & Thompson, M. J. 2000, *Sol. Phys.*, 192, 437
- Vorontsov, S. V., Christensen-Dalsgaard, J., Schou, J., Strakhov, V. N., & Thompson, M. J. 2002, *Science*, 296, 101
- Wang, Y.-M., Lean, J. L., & Sheeley, N. R. 2005, *ApJ*, 625, 522
- Wang, Y. M. & Sheeley, N. R. 1991, *ApJ*, 375, 761
- Yoshimura, H. 1981, *ApJ*, 247, 1102
- Zhao, J. & Kosovichev, A. G. 2004, *ApJ*, 603, 776